Available online at www.sciencedirect.com
ScienceDirect
Journal of Nuclear Materials 363–365 (2007) 319–324
journal of nuclear materials
www.elsevier.com/locate/jnucmat

ELM-wall interaction on JET and ITER

W. Fundamenski [a,*], R.A. Pitts [b], JET EFDA contributors [1]

[a] Euratom/UKAEA Fusion Association, Culham Science Centre, Abingdon, OX14 3DB, UK
[b] CRPP, Assoc. Euratom-EPFL, CH-1015, Lausanne, Switzerland

Abstract

Significant interaction of ELM filaments with the vessel wall is now observed on JET by several diagnostics. To interpret the experimental data, a model of ELM-filament evolution was developed, with the radial velocity taken from experiment and the decay of filament density and temperature calculated based on parallel losses to the divertor targets. The model was found to successfully reproduce radial e-folding lengths of density, electron temperature and energy, λ_n^{ELM}, $\lambda_{T_e}^{ELM}$ and λ_W^{ELM}, inferred from dedicated outer gap-scan experiment for moderate Type-I ELMs ($\Delta W/W \sim 5\%$, where W is the plasma stored energy). It also showed excellent agreement with observations of far SOL ELM ion energies on JET. For nominal ITER conditions (4 keV pedestal, 5 cm outer gap), the same model predicts that ~8% of the ELM energy would be deposited on the main chamber wall (mostly on the upper X-point blanket modules), with the ions carrying most of this power and striking the wall tiles with an impact energy in excess of 1 keV.

PACS: 52.30.−q; 52.40.Hf; 52.55.Fa; 52.55.Rk

Keywords: ELM; Divertor; JET; ITER; Power deposition

1. Introduction

The interaction of edge localised modes (ELMs), or more accurately of ELM plasma filaments, with the tokamak first wall (divertor and limiter tiles) is one of the critical issues for ITER. Specifically, the heat fluxes deposited on the limiter tiles by the ELM filaments are of great practical importance. This article presents a brief overview of what we know and understand regarding the interaction of ELM filaments with the main chamber wall on JET, and by inference on ITER. Unless otherwise stated, Type-I ELMs will be assumed.

2. ELM filament measurements on JET

An early indication of ELM-wall interaction on JET was obtained by subtracting two visible images of main chamber recycling, thus revealing the interaction with outboard limiters and upper baffle, as well as a faint but visible helical stripe [1]. Such field aligned helical features were also recently observed on the main wall using the wide angle infrared camera. Moreover, infrared thermography on the divertor target showed that up to half of the ELM energy

* Corresponding author. Fax: +44 1235 464882.
E-mail address: wfund@jet.uk (W. Fundamenski).
[1] See appendix of J. Pamela, Fusion Energy 2004 (Proc. 20th Int. Conf. Vilamoura, 2004) IAEA, Vienna (2004).

0022-3115/$ - see front matter © 2007 Published by Elsevier B.V.
doi:10.1016/j.jnucmat.2007.01.272

was missing from the divertor, and was presumably lost to the wall [2,3].

Later, ELM filaments were detected on outboard limiters using embedded Langmuir probes [4]. The SOL-average radial velocity of the filaments was measured as ~600 m/s, and their radial expansion was characterised as ~500 m^2/s. The filaments were also shown to be quite cool, $T_e \sim 25$ eV, compared to the pedestal temperature of ~1 keV, and quite dilute, with a drop in density by a factor of 10. Their radial e-folding lengths of density and temperature were inferred as 50 and 30 mm, respectively. Since the wall gap (the closest distance between the separatrix and the wall) was quite large in these discharges (>10 cm), power balance indicated that only ~5% of the ELM energy was deposited on the limiters.

ELM filaments were also measured by a turbulence triple probe mounted on a fast scanning, reciprocating assembly near the top of the torus [5,6]. Indeed, filamentary fine structures were observed in both the particle flux and the electron temperature. The radial velocities were again measured in the range of 1 km/s and the filaments were found to be relatively cold, $T_e \sim 30$ eV.

ELM filament ion energies were measured by a Retarding Field Analyser probe head mounted on the same reciprocating assembly [6]. Coherent spikes were observed in both the plasma flux and hot ion flux and were interpreted as the arrival of interspaced, toroidaly rotating filaments. The ratio of ion and electron side fluxes indicated a parallel plasma flow to the inboard side, consistent with the filament entering the SOL on the outboard side and launching a sound wave disturbance along the field lines. Filament ion temperature was inferred as ~100 eV, compared to ~400 eV at the pedestal [6,7]. Successive filaments were found to carry less energy and to persist for 2 ms, or roughly ten times longer than the duration of the ELM determined from magnetic signals.

To investigate the total power transported by these filaments to the limiters, dedicated experiments were recently performed in which the (outer) wall gap was reduced while the strike point position on the divertor was held fixed, Fig. 1 [8]. Based on IR measurements of power deposition on divertor targets, the radial e-folding lengths for moderate ($\Delta W/W \sim 5\%$) Type-I ELMs were inferred as 35 mm for the filament average energy, and 24 mm for the peak energy. These values were confirmed, to within 10%, based on divertor thermocouple measurements. Note that variation of ELM size with wall gap, which showed a positive correlation, was taken into account in the analysis.

3. Interpretation and extrapolation to ITER

To interpret these various observations, it is helpful to introduce a three stage picture of the ELM event, as represented schematically in Fig. 1 in [7]. The first stage represents the growth of some MHD instability, eg. the Peeling–Ballooning mode, which forms ~10–20 ripples in thermodynamics quantities. In the second stage, the instability grows non-linearly and saturates due to transport (or drift-ordered) effects, forming ~10–20 plasma filaments. At this stage, reconnection may also occur in the X-point region, forming a new separatrix. Finally, in the exhaust stage, the filaments move outwards due to interchange forces and expand by breaking up into ever smaller structures. They also experience strong parallel losses to the divertor targets, such that their particle, energy and current content is quickly depleted.

Plasma filaments may either move with or drift across magnetic field lines, the former process corresponding to MHD-ordered, the latter to drift-ordered motions [9]. The most likely mechanism for the latter process is radial interchange motion, in which the filament is accelerated due to a combination of ion inertia and magnetic curvature, that is, polarisation of charge [10]. The filament then breaks up into two counter-rotating lobes, developing the characteristic mushroom shape, and forms a leading front and a trailing wake [11].

As the filaments evolve, at some point they must begin to lose their particle, energy and current content to the divertor targets; below we define $t = 0$ as the time at which such parallel losses begin. In the absence of reconnection, this occurs when the filament reaches the separatrix location, whereas if reconnection is present from the outset, $t = 0$ corresponds to the pedestal location. More generally, one may assume that parallel losses begin at some mid-pedestal position.

A simplified description of the ELM filament may be obtained by considering the conservation equations of mass and energy, together with parallel losses. The Green's function of these equations, that is the response to a delta function impulse, yields a field-aligned, advective–diffusive, gaussian wave-packet [7], which is the lowest order description of the plasma filament. Its integral falls exponentially due to parallel losses, while the peak value is addi-

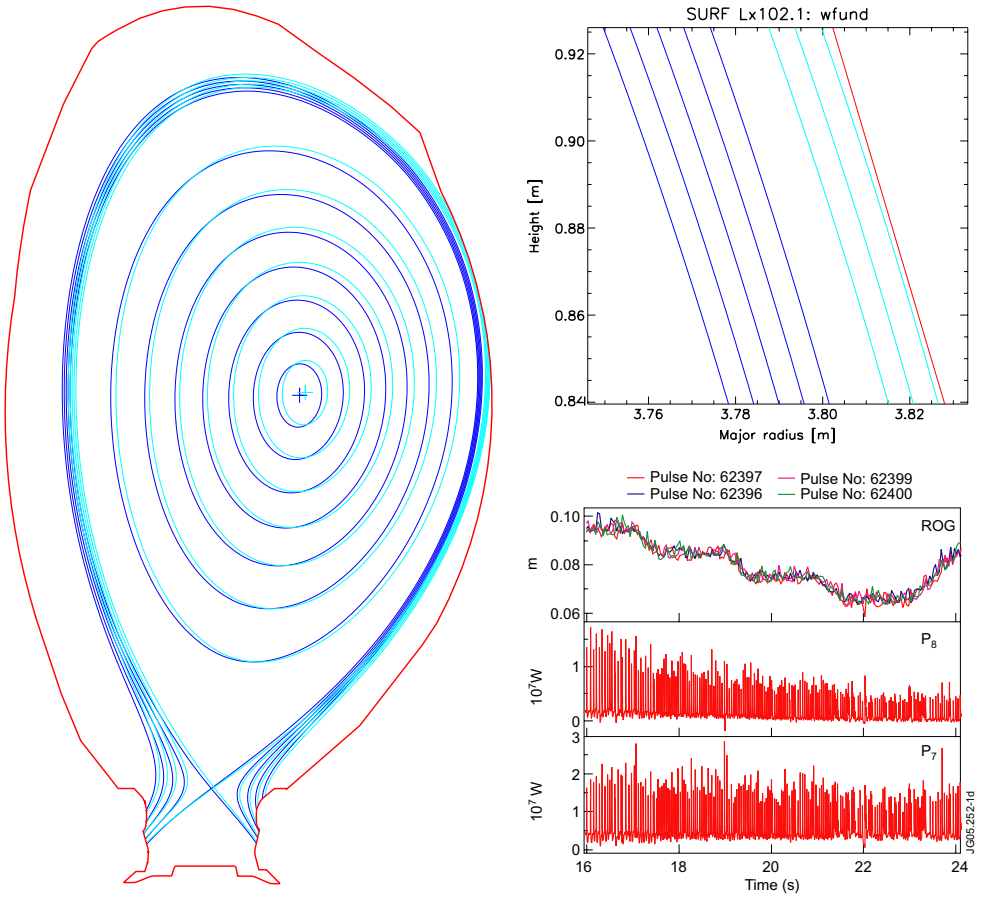

Fig. 1. Magnetic equilibria for largest and smallest outer gap (left), magnified region of closest approach to the limiter (right top), and time traces of the separatrix-limiter gap at the outer mid-plane (ROG) and IR measured power on upper (P_8) and lower (P_7) outer vertical tiles for a natural density H-mode (right bottom). Spacing between magnetic surfaces is 1 cm at outer mid-plane.

tionally reduced due to filament broadening. It is convenient to separate these two effects, first calculating the drop in the integral and peak quantities in the absence of radial expansion, then estimating the reduction in the peak value assuming semi-adiabatic expansion [7].

The temporal evolution of the former in the filament frame of reference can be obtained by averaging the conservation equations of mass and energy over the filament, which yields the following simple fluid based model (a kinetic version of the model has also been developed but is not discussed here) [7]:

$$\begin{aligned}
&\left(\frac{\partial}{\partial t}+\frac{1}{\tau_{\mathrm{n}}}\right)n = S_{\mathrm{n}},\\
&\left(\frac{\partial}{\partial t}+\frac{1}{\tau_{\varepsilon,\mathrm{i}}}\right)\varepsilon_{\mathrm{i}}+\frac{\varepsilon_{\mathrm{i}}-\varepsilon_{\mathrm{e}}}{\tau_{\mathrm{ie}}^{\mathrm{eq}}} = S_{\mathrm{i}},\\
&\left(\frac{\partial}{\partial t}+\frac{1}{\tau_{\varepsilon,\mathrm{e}}}\right)\varepsilon_{\mathrm{e}}-\frac{\varepsilon_{\mathrm{i}}-\varepsilon_{\mathrm{e}}}{\tau_{\mathrm{ie}}^{\mathrm{eq}}} = S_{\mathrm{e}},
\end{aligned} \tag{1}$$

where n and $\varepsilon_{\mathrm{a}} = (3/2)nT_{\mathrm{a}}$ represent characteristic (peak or average) particle and energy densities of the filament in the absence of radial expansion. Parallel losses are treated with diffusive and advective removal times, τ_{n}, $\tau_{\varepsilon,\mathrm{i}}$ and $\tau_{\varepsilon,\mathrm{e}}$, and the two temperatures are coupled by the ion–electron equilibration time, $\tau_{\mathrm{ie}}^{\mathrm{eq}}$; for definition all these times see Eq. (5.3) in Ref. [7]. It is important to note that time and radius are related by the filament radial velocity, which is prescribed within the model. Thus the density is removed roughly at the plasma sound speed, $\tau_{\mathrm{n}} = L_{\parallel}/Mc_{\mathrm{s}}$, while energy is removed by a combination of convection and conduction, which is much faster for electrons than for ions.

Typical evolution of n, T_{e} and T_{i}, normalised by their initial values (we denote these normalised quantities with a prime, e.g. $n' = n/n_0$), for JET are shown in Fig. 2 for two initial values of the filament density; the results are obtained by solving

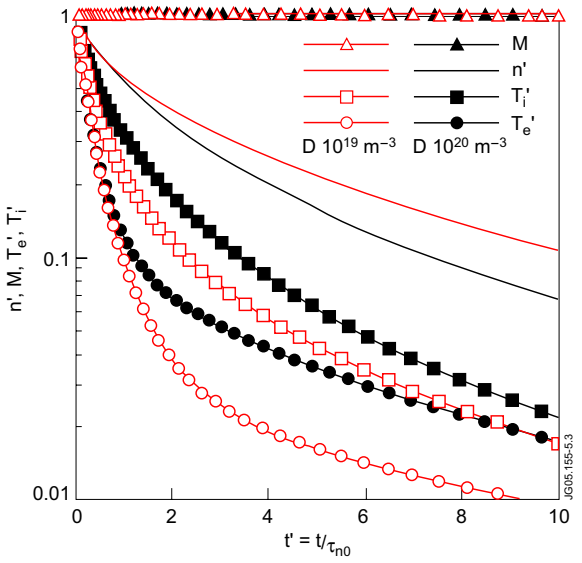

Fig. 2. Evolution of ELM filament particle density, n, Mach number, M, electron and ion temperatures, T_e and T_i, normalised to their initial values, as a function of the time since the start of parallel losses, normalised by the initial density removal time, $\tau_{n0} = L_{\parallel}/c_{s0}$. The plot refers to typical JET conditions at two values of the initial density.

equation set (1) using a forward marching numerical scheme. As expected, one typically finds that electron temperature decays fastest, followed by the ion temperature and the density; that is the electrons are cooled much faster than ions. The ion-to-electron temperature ratio, which reaches a maximum of ~3–5 after several sonic transit times. As the initial filament collisionality is increased, electron-ion energy exchange becomes more effective and the two temperatures converge more quickly. In the second stage of the model, the reduction in the above due to filament broadening is estimated by assuming semi-adiabatic ($T \propto n^{\gamma-1} \propto n^{1/3}$) expansion and $n_\gamma/n = n_{max}/n = \Delta_{ped}/(\Delta_{ped} + \Delta_{SOL}) < 1$, where Δ_{ped} and Δ_{SOL} are the radial widths of the pedestal and SOL (separatrix-wall gap), respectively. The subscript 'max' refers to the final prediction of the peak filament quantity.

The model was first used to interpret the RFA measurements. The radial velocity was taken from experiment at 600 m/s, the mid-pedestal approximation was adopted and the filament was assumed to expand semi-adiabatically. These predictions are in excellent agreement with the experimental data, and reproduce both the peak plasma flux to the probe and the peak hot ion flux, that is the ion energy. The model was then applied to the limiter probe and outer gap scan experiments with the results shown in Table 1. The density and electron temperatures at the limiter probe, and hence the average e-folding lengths of these quantities, are reproduced quite well. Likewise, the measured energy e-folding lengths agree quite well with model predictions. Finally, the model is consistent with the energy deficit based in small wall gap configurations (~3 cm) [2,3] which indicate ~30% missing power for moderate ($\Delta W/W \sim 5\%$, $\Delta W/W_{ped} \sim 12\%$) Type-I ELMs, see Fig. 11 in [3]. This value is consistent with the observed and predicted ELM

Table 1
Comparison between experimental measurements and parallel loss model predictions of ELM-wall contact on JET in four separate dedicated experiments

Experiment	Parallel loss model
Limiter probes + TC	
$T_e(r_{lim}) \sim 25$–30 eV,	$T_e(r_{lim}) \sim 30$ eV
$n_e(r_{lim}) \sim 2.4 \times 10^{18}$ m^{-3}	$n_e(r_{lim}) \sim 2.2 \times 10^{18}$ m^{-3}
$\lambda_{n,max} \sim 50$ mm, $\lambda_{T_e,max} \sim 30$ mm	$\lambda_{n,max} \sim 47$ mm, $\lambda_{T_e,max} \sim 32$ mm
Nearly all power found on the divertor	Fraction of ELM energy to limiter ~5%
Outer gap scan + IR and TC	
$\lambda_W \sim 33$–35 mm, $\lambda_{W,max} \sim 22$–24 mm	$\lambda_W \sim 36$ mm, $\lambda_{W,max} \sim 22$ mm
RFA measurements of ion energies	$T_{i,max}(r_{lim}) \sim 100$ eV,
$J_{sat,max} \sim 2$ A cm^{-2}	$T_{e,max}(r_{lim}) \sim 40$ eV,
$I_{coll,max} \sim 100$ μA	$n_e(r_{lim}) \sim 4.3 \times 10^{18}$ m^{-3}
(reproduced by model)	$\lambda_{n,max} \sim 48$ mm, $\lambda_{T_i,max} \sim 52$ mm
	$\lambda_{T_e,max} \sim 30$ mm, $\lambda_W \sim 32$ mm
	Fraction of ELM energy to limiter ~15%
ELM energy deficit based on IR	
~30% for ~3 cm gap and $\Delta W/W \sim 5\%$	~30% based on $\lambda_W^{ELM} \sim 35$ mm

energy e-folding length of $\lambda_W^{ELM} \sim 35$ mm combined with the mid-pedestal approximation, i.e. $\exp[-(30+15)/35] \sim 28\%$. Overall, the level of agreement is impressive, even surprising, considering the approximate nature of the model.

Assuming that ELM filaments are driven by interchange motions, one expects more intense filaments to travels faster, such that the variation with ELM amplitude to scale roughly as $\lambda_W/L_\parallel \sim v_\perp/c_s \sim (\Delta p/p)^{1/2} \sim (\Delta W/W)^{1/2}$ [11]. This result is consistent with the observation that larger ELMs lose more energy to the wall [2,3] and allows us to construct an expression for the ELM filament energy e-folding length on JET, $\lambda_W^{ELM-JET} \sim 35[(\Delta W/W)/0.05]^{1/2}$ mm, which should be used with the mid-pedestal width. The fraction of ELM energy deposited on the wall is then found as $(W_{wall}/W_0)^{ELM-JET} = \exp\left[-(\Delta_{ped}/2+\Delta_{SOL})/\lambda_W^{ELM-JET}\right]$, where W_0^{ELM} is the initial energy content of the filament and W_{wall}^{ELM} the energy which it deposits on the wall.

The next logical step is to predict the degree of ELM-wall interaction on ITER. This was done using the same prescription as was used to match the JET data, with the radial velocity extrapolated from JET based on the sheath-limited blob theory [12]. The results are shown in Fig. 3 where the shaded region indicates the location of the 2nd separatrix at the upper X-point blanket models. In the ITER reference scenario [13], this point of largest plasma-wall contact is located at 5 cm away from the separatrix near the top of the torus. The model predicts 8% of the ELM energy to be deposited on the main wall with a peak electron temperature of 140 eV, peak ion temperature of 350 eV, peak impact energy of $\approx 3T_e + 2T_i \approx 1.1$ keV, the peak parallel plasma flux $\Gamma_{\parallel max} = nc_s \approx 2\times 20^{24}$ m^{-2} s^{-1} and peak parallel heat flux of $q_{\parallel max} = (5T_e + 2T_i)\Gamma_{\parallel max} \approx 400$ MW/m^2, although the last quantity may be larger due to transiently higher values of γ_e and γ_i. Peak ELM filament quantities at the

Table 2
Summary of predicted peak ELM filament quantities, including semi-adiabatic expansion ($\gamma = 4/3$), at the nominal limiter radii for JET and ITER, such that $n_{max}/n \approx 0.5$ and $n_{max}/n \approx 0.8$. Here $\Gamma_{\parallel max} = nc_s$ and $q_{\parallel max} = (5T_e + 2T_i)\Gamma_{\parallel max}$

	JET	ITER
n_{max} (m^{-3})	8.25×10^{18}	1.2×10^{19}
$T_{i,max}$ (eV)	185	350
$T_{e,max}$ (eV)	74	140
$\Gamma_{\parallel max}$ (m^{-2} s^{-1})	9×10^{23}	1.8×10^{24}
$q_{\parallel max}$ (MW m^{-2})	110	410
$\lambda_{n,max}$ (mm)	47	54.5
$\lambda_{T_i,max}$ (mm)	41	42.5
$\lambda_{T_e,max}$ (mm)	25	27.5

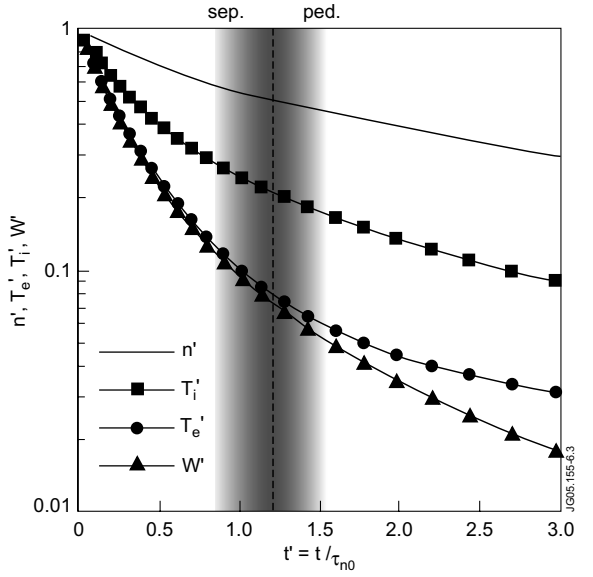

Fig. 3. Predicted normalised ELM filament quantities in ITER as a function of normalised time since the start of parallel losses; here W' is the energy content of the filament normalised by its initial value. The vertical bar represents the uncertainty in the transit time of the filament to the wall.

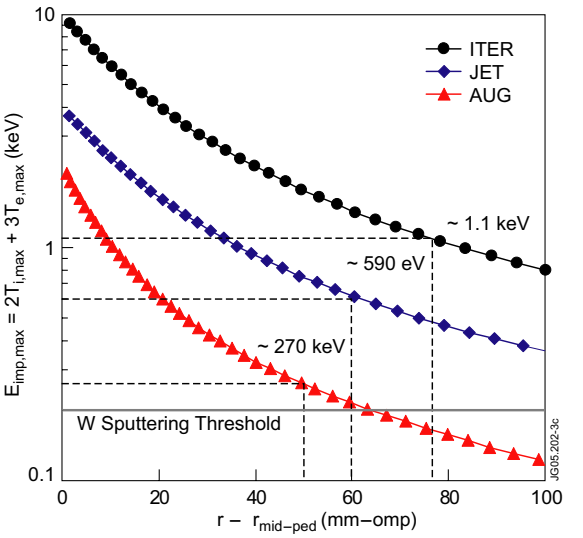

Fig. 4. Predicted peak ion impact energy, including semi-adiabatic expansion, as a function of radial distance from the mid-pedestal position on AUG, JET and ITER [7] for moderate ELMs.

point of first wall contact, are shown in Table 2, along with average e-folding lengths of density and temperatures, and corresponding JET values which are included for comparison; note that in all three cases the model predicts that $\lambda^{\mathrm{ITER}} \approx \lambda^{\mathrm{JET}}$. It also predicts that only 1.5% of the ELM energy reaches the limiter location, a further 10 cm into the SOL [7]. For wall gaps smaller than 5 cm, the fraction of ELM energy to the wall can be approximated as $\lambda_{\mathrm{W}}^{\mathrm{ELM-ITER}} \sim 30[(\Delta W/W)/0.05]^{1/2}$ mm, which should likewise be used with $\Delta_{\mathrm{ped}}/2$; this estimate likely represents a lower bound on the actual values. The predicted ion impact energies due to moderate Type-I ELM filaments contact with the wall as a function of radial distance away from the mid-pedestal location on ASDEX-Upgrade (AUG), JET and ITER are shown in Fig. 4. Note that, under most conditions, the tungsten sputtering threshold, indicated by a horizontal grey line, is significantly exceed on both JET and ITER.

4. Conclusions

ELM filaments are now observed on JET by several diagnostics and show significant interaction with main chamber wall and limiters. All ELM-limiter interaction data on JET can be reproduced with the parallel loss model. Extrapolating to ITER for moderate ($\Delta W/W \sim 5\%$) Type-I ELMs, the model predicts that ~8% of the energy to be deposited on the main wall and ~1.5% on the outboard limiter in a reference ITER scenario. For wall gaps, Δ_{SOL}, smaller than 5 cm, the fraction of ELM energy to the wall on ITER is estimated as $(W_{\mathrm{wall}}/W_0)^{\mathrm{ELM-ITER}} = \exp\left[-(\Delta_{\mathrm{ped}}/2 + \Delta_{\mathrm{SOL}})/\lambda_{\mathrm{W}}^{\mathrm{ELM-ITER}}\right]$, where $\lambda_{\mathrm{W}}^{\mathrm{ELM-ITER}} \sim 30[(\Delta W/W)/0.05]^{1/2}$ mm, mapped to the outer mid plane.

Acknowledgements

This work was partly funded by the United Kingdom Engineering and Physical Sciences Research Council and by the European Communities under the contract of Association between EURATOM and UKAEA. The views and opinions expressed herein do not necessarily reflect those of the European Commission. This work was carried out within the framework of the European Fusion Development Agreement.

References

[1] Ph. Ghendrih et al., J. Nucl. Mater. 313–316 (2003) 914.
[2] T. Eich et al., J. Nucl. Mater. 337–339 (2005) 669.
[3] A. Loarte et al., Phys. Plasma 11 (2004) 2668.
[4] W. Fundamenski et al., Plasma Phys. Contr. Fusion 46 (2004) 233.
[5] C. Silva et al., J. Nucl. Mater. 337–339 (2005) 722.
[6] R.A. Pitts et al., Nucl. Fusion 46 (2006) 82.
[7] W. Fundamenski et al., Plasma Phys. Contr. Fusion 48 (2006) 109.
[8] W. Fundamenski et al., in: Proceedings of the 32nd EPS Conference on Plasma Physics, Tarragona, Spain, 2005 29C, P2.013.
[9] W. Fundamenski et al., Plasma Phys. Contr. Fusion, in press.
[10] O.E. Garcia et al., Phys. Plasma 12 (2005) 090701.
[11] O.E. Garcia, N.H. Bian, W. Fundamenski, Phys. Plasmas 13 (2006) 082309.
[12] D.A. D'Ippolito et al., Phys. Plasmas 9 (2002) 222.
[13] R. Aymar et al., Plasma Phys. Contr. Fusion 44 (2002) 519.